Thermoelectric properties of La7Mo7O30 sintered by reactive spark plasma sintering

F. Giovannelli, E. Sabarthes, F. Delorme

Version of Record: https://www.sciencedirect.com/science/article/pii/S0272884222044352
Manuscript_61e0082a123428a41da59ece0a36c12a

Thermoelectric properties of $La_7Mo_7O_{30}$ sintered by reactive spark plasma sintering

F. Giovannelli*, E. Sabarthes, F. Delorme

GREMAN UMR 7347, Université de Tours, CNRS, INSA CVL, IUT de Blois, 15 rue de la chocolaterie, CS 2903, F-41029 Blois Cedex, France.

*** corresponding author**

Abstract

In this work, spark plasma sintering of $La_2Mo_2O_9$ powder was used to achieve dense ceramics of $La_7Mo_7O_{30}$ and explore their thermoelectric properties. SPS sintering of $La_2Mo_2O_9$ powder at 973 K for 10 minutes under 90 MPa leads to a bicoloured sample with white and black faces. XRD patterns of white and black faces are attributed to $La_2Mo_2O_9$ and $La_7Mo_7O_{30}$ phases, respectively. These experimental conditions allow observing the in-situ reduction of $La_2Mo_2O_9$ during the SPS process. With a longer sintering time of 30 minutes, a ceramic of $La_7Mo_7O_{30}$ is obtained. Its electrical conductivity exhibits a semiconducting behaviour and reaches a value of 1000 Sm^{-1} at 1000 K. The negative Seebeck coefficient show a n-type conduction in this phase. $La_7Mo_7O_{30}$ exhibits a very low thermal conductivity, less than 1 $Wm^{-1}K^{-1}$ from room temperature up to 1000 K, similar to the values reported for $La_2Mo_2O_9$. A figure of merit of 0.04 is reached at 1000 K.

Keywords : Thermoelectrics ; Thermal conductivity ; Oxide, Reactive Spark Plasma Sintering

Introduction

To reduce energy consumption, the recovery of wasted energy in the form of heat via a thermoelectric module is a promising solution. However, materials used in commercially available thermoelectric modules are expensive and not widely available on Earth, which does not allow for a large-scale use of thermoelectricity. Transition metal oxides, thus, have several advantages for thermoelectric applications, including their stability in air at high temperatures and the high abundance of their constituents [1, 2]. Since the discovery by Terasaki et al. [3] of a high power factor in Na_xCoO_2, an intensive search for new thermoelectric oxides is taking place [4-24]. Some oxides can exhibit a power factor comparable to that of other classes of thermoelectric materials. For instance, the power factor of $SrTiO_3$ ceramics substituted with a trivalent element on the A-site of the perovskite is similar to that of Bi_2Te_3 (> 10^{-3} $Wm^{-1}K^{-2}$) [25-28]. However, the thermal conductivity is much higher for $SrTiO_3$ (> 5 $Wm^{-1}K^{-1}$) than for Bi_2Te_3 (< 2 $Wm^{-1}K^{-1}$). The thermal conductivity is therefore generally too high in oxides and does not allow for competitive figures of merit.

Different strategies have been investigated such as nanostructuration [29-32], composites [33- 35], introduction of porosity [36-38], complex crystal structures [39-42], to decrease the

thermal conductivity in thermoelectric oxides. Another strategy, in order to obtain an efficient thermoelectric material, is to consider a material with an intrinsically low thermal conductivity. $La_2Mo_2O_9$ has one of the lowest thermal conductivities among crystalline oxides ($\kappa < 1$ $Wm^{-1}K^{-1}$) [43, 44]. However, no study has been done on its thermoelectric properties due to its low electronic conductivity [45, 46]. The challenge for this compound is then to increase its electrical conductivity. In transition metal oxides, a common route is the reduction of the transition metal through annealing treatments [47]. $La_2Mo_2O_9$ has been studied mainly in the context of the development of solid electrolytes for fuel cells due to its exceptionally high ionic conductivity at high temperatures [48]. This structure can accept different oxygen contents. The partial reduction of $La_2Mo_2O_9$ leads successively to a crystallized phase with the same structure but with a lower oxygen content ($La_2Mo_2O_{8.96}$), then a crystallized phase with a different structure ($La_7Mo_7O_{30}$) and finally an amorphous phase ($La_2Mo_2O_{7-y}$). Electrical transport studies suggest that $La_2Mo_2O_{8.96}$ has a mixed ionic and electronic conductivity [49]. Partial reduction of the compound induces a molybdenum oxidation state of +5.96 allowing the activation of electronic transport [49]. In the case of $La_7Mo_7O_{30}$, two molybdenum sites valences of +4.5 and +5.75, respectively, are present in the structure [50]. A non-negligible electronic conductivity is therefore expected, which could give rise to promising thermoelectric properties. The stacking structure of $La_7Mo_7O_{30}$ is, moreover, assimilated to a one-dimensional structure and the structures of low dimensionality can induce peaks in the density of state close to the Fermi level resulting in an increased Seebeck coefficient [13, 51, 52]. Reduced $La_2Mo_2O_9$ derivatives are generally obtained by heat treatment in a reducing atmosphere [50, 53]. Nowadays, the only known protocol to obtain ceramics of these compounds is to reduce previously sintered $La_2Mo_2O_9$ ceramics. Unfortunately, the reduction of the pellets inevitably creates cracks in the microstructures due to the departure of oxygen [54]. Reduced oxides have been obtained directly by Spark Plasma Sintering (SPS) leading to electrical conductivity in dielectric material [55]. Moreover, in the case of W-O system, the reduced phase WO_x ($2.50 < x < 3$) could be directly synthesized by reactive SPS from WO_3 and W [56].

Therefore, in order to avoid cracks formation inherent to the annealing of $La_2Mo_2O_9$ ceramics in a reducing atmosphere, this work proposes to directly reduce $La_2Mo_2O_9$ during the sintering by SPS in order to achieve dense ceramics and then explore the thermoelectric properties of such $La_7Mo_7O_{30}$ reduced pellets.

Materials and methods

$La_2Mo_2O_9$ powder was prepared by conventional solid-state reaction starting from a stoichiometric mixture of La_2O_3 (99.99 %) and MoO_3 (99.9 %) from ChemPur. Prior to use, La_2O_3 was calcined in air for 10 h at 1273 K to remove adsorbed water and carbon dioxide. The mixture of elementary oxides was manually grounded in an agate mortar and the resulting powder was shaped into pellets (16mm in diameter) at 160 MPa by uniaxial cold-pressing. Three successive thermal cycles were necessary to synthesize pure phases. Pellets were first heated up at 873 K and at 973 K during 12h with a heating rate of 2 $K.min^{-1}$ and a cooling rate of 5 $K.min^{-1}$ in order to avoid molybdenum sublimation [57] Pellets were then calcined at 1173 K during 12 h with a 5 $K.min^{-1}$ heating and cooling rate. Between each step, the resulting

pellets were manually ground in an agate mortar and shaped into pellets at 160 MPa. Sintering was performed using a spark plasma sintering apparatus (Syntex 515S- FUJI). Powder was loaded into a cylindrical graphite die of 15 mm. In order to remove the sample easily from the graphite die and to ensure a good electrical contact, a graphite foil was placed between the powder and the graphite tools (die and punches). The heating rate was 100K min^{-1} up to the sintering temperature of 973K. Temperature was maintained for 5 or 30 min under a uniaxial pressure of 90 MPa in Ar atmosphere. During the sintering process, the temperature was recorded with a thermocouple.

Phase purity of raw pellets was checked by recording X-ray diffraction patterns at room temperature on a Brücker D8 Advance θ–2θ Bragg–Brentano diffractometer ($CuK_{\alpha 1+2}$ radiations, Cu-anode operating at 40 kV and 40 mA) equipped with a Lynxeye energy-dispersive one-dimensional detector. The diffractograms were collected on the surface of pellets in the [10–80°] scattering angle 2θ range with a 0.02° step for a total acquisition time of 1 h.

Scanning electron microscope (SEM) observations have been performed using a FEI Nova NanoSEM 450 field emission SEM. Thermoelectric measurements on bar-shaped samples (3 x 3 x 12 mm^3), including the electrical conductivity and the Seebeck coefficient, were simultaneously measured in the temperature range 400-1000K using an ULVAC ZEM-3 equipment. Thermal diffusivity measurements of parallelepipedal specimens (6 x 6 x 1 mm^3) were carried out using a laser flash system (Netzsch LFA 457) in vacuum. Three measurements were conducted at each temperature, between 400 and 1000K, to assess reproducibility. Both surfaces were coated with a thin layer of graphite to increase the absorption of infrared radiation energy. Specific heat capacity measurements were carried out by Differential Scanning Calorimeter (DSC, Netzsch STA 449 F3 Jupiter) in a continuous-heating mode of 20 K min^{-1} up to 1000 K using 50 mg of powdered sample introduced into platinum crucibles.

Results and discussion.

A first SPS trial starting with $La_2Mo_2O_9$ powder at 973 K for 10 min under a pressure of 90 MPa led to a bicoloured sample with a white top face and a black bottom face. XRD patterns of both faces show structural differences (figure 1). The diffraction peaks on the white face correspond mostly to the $La_2Mo_2O_9$ phase (PDF 01-074-3327) and those on the black face to $La_7Mo_7O_{30}$ (PDF 00-050-1866). The white face also exhibits some low intensity diffraction peaks, corresponding to the reduced phase, and resulting from the transformation of $La_2Mo_2O_9$ into $La_7Mo_7O_{30}$ by reduction during the SPS sintering cycle. Diffraction peaks of residual $La_2Mo_2O_9$ are similarly observed on the black face pattern with notably the presence of a peak at 47.5°2θ that indicates that the reduction is not completed. The color change could be related to oxygen deficiency due to reducing atmosphere of SPS leading to $La_2Mo_2O_{9-\delta}$. Buvat et al. have shown that $La_2Mo_2O_9$ is transformed during an isothermal treatment at 881K and 991K in, respectively, $La_2Mo_2O_{8.96}$ and $La_7Mo_7O_{30}$, when the partial pressure of oxygen decreases [53]. The sintering temperature in SPS is 973K, which is consistent with the presence of $La_7Mo_7O_{30}$ detected by X-ray diffraction. Therefore, the SPS process could explain the color difference between the two faces. SPS heating is due to DC current pulses that gradually heat the graphite die. A precise control of the current and the voltage is used to ensure the

requested thermal profile. In Syntex 515S- FUJI apparatus, the electric field is always applied in the same direction from the top to the bottom face of the pellet. As $La_2Mo_2O_9$ is an ionic conductor [48], oxygen moves during sintering from the black face up to the white face leading to the reduction of $La_2Mo_2O_9$ in $La_7Mo_7O_{30}$. A similar behaviour has recently been reported in KNN ceramics sintered by SPS, but in a lesser extent [58]. In these conditions, a full reduction of $La_2Mo_2O_9$ could be possible with longer high temperature dwell times.

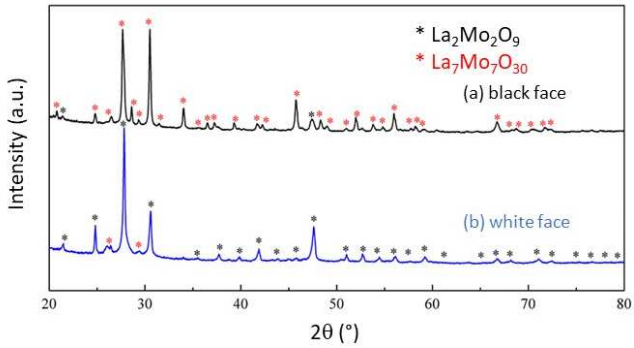

Figure 1: XRD patterns of $La_2Mo_2O_9$ powder sintered by SPS at 973 K during 10 minutes.

Figure 2 shows diffraction patterns of samples obtained after a high-temperature dwell time of 30 and 60 minutes. Both patterns are similar and the reduced phase $La_7Mo_7O_{30}$ is predominantly detected. Although completely black, both samples show a residual $La_2Mo_2O_9$ phase responsible for the low intensity diffraction peak at 47.5°2θ. However, there is one major difference between the two samples: the 30 minutes cycle results in a structurally dense and stable pellet, whereas the 60 minutes cycle sample is extremely fragile and brittle and comes out of the SPS die in several pieces. The most likely explanation for this is that the further reduction of the $La_7Mo_7O_{30}$ phase leads to the formation of the amorphous $La_2Mo_2O_{7-\delta}$ phase on the surface of the grains, which affects the cohesion of the ceramic. Buvat et al. [53] described the mechanism for reduction of $La_2Mo_2O_9$ during annealing in a reducing atmosphere where $La_7Mo_7O_{30}$ serves as an intermediate phase for the formation of the amorphous phase.

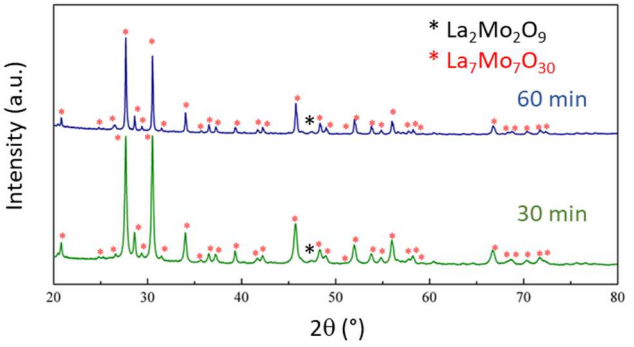

Figure 2: XRD pattern of La2Mo2O9 powder sintered by SPS at 973 K during 30 and 60 minutes.

The ceramic obtained after the 30 minutes cycle has a relative density of 89% (the presence of $La_2Mo_2O_9$ impurity has not been taken into account in the calculation of the relative

density). The microstructure exhibits some porosity, consistent with the relative density value, and grains of a few microns (figure 3).

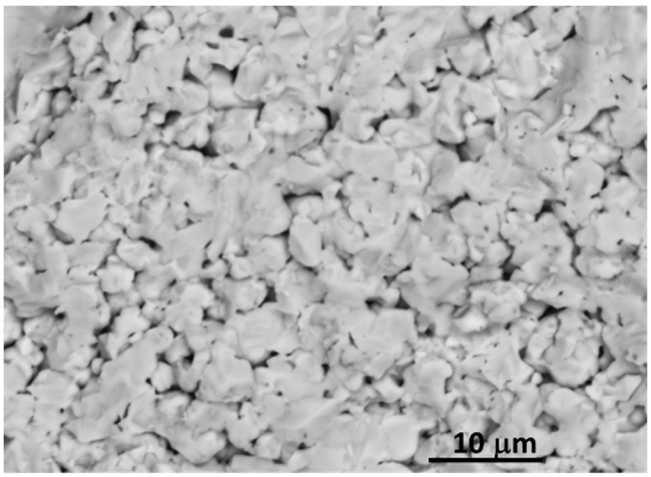

Figure 3: SEM Image of the ceramic sintered by SPS at 973 K during 30 minutes

The electrical conductivity increases with temperature (from ~10 $S.m^{-1}$ at 373 K to ~10^3 $S.m^{-1}$ at 973 K), reflecting the semiconducting nature of the reduced $La_7Mo_7O_{30}$ phase (figure 4). The possible contribution to the electrical transport of the residual $La_2Mo_2O_9$ phase is necessarily negligible given its low conductivity (~10^{-1} $S.m^{-1}$ from 773 to 973 K) [48].

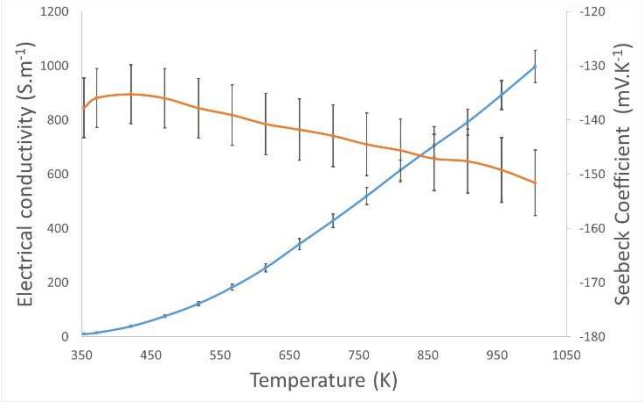

Figure 4: Temperature dependence of electrical conductivity and Seebeck coefficient of $La_7Mo_7O_{30}$ ceramic.

Given the ionic nature of lanthanum molybdate, the electrical conductivity was examined in terms of the small polaron hopping model (Figure 5) to determine the gap energies of the compounds [59]:

$$\sigma = \frac{\sigma_0}{T} e^{\frac{-E_a}{k_b T}}$$

where σ, σ_0, k_b and E_a are respectively the electrical conductivity, a constant, the Boltzmann constant and the activation energy.

This model adequately describes the electrical transport above 473 K and the calculated activation energy (E_a) is equal to 254 meV.

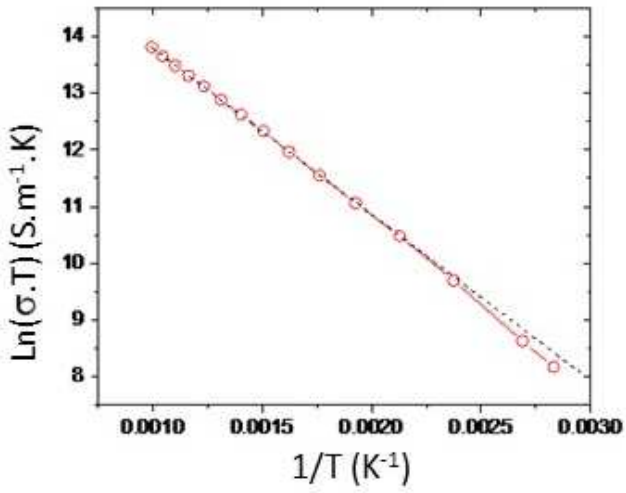

Figure 5: Plot of Ln(σT) versus 1/T with data of figure 4. The dash lined correspond to the small polaron hopping model.

The Seebeck coefficient of the compound versus temperature is shown in Figure 4. The negative sign of the Seebeck coefficient indicates that $La_7Mo_7O_{30}$ is an n-type semiconductor. The absolute value of the Seebeck coefficient first slightly decreases from room temperature to 473K, and then increases with temperature from 473 to 1000K. The temperature at which this behaviour change is observed coincides with the change in electrical behaviour (figure 5). In $La_7Mo_7O_{30}$, the charge carrier concentration depends on the relative proportion of Mo^{IV}, Mo^{V} and Mo^{VI}. With temperature increase, the energy barrier associated with electron hopping from Mo^{IV} and Mo^{V} to an adjacent site of Mo^{V} and Mo^{VI} is easily overcome. As the probability of hopping increases, the mobility of charge carriers increases leading to an improvement of the electrical conductivity. In the case of the hopping regime, the Seebeck coefficient can be described by the modified Heikes equation [60, 61]:

$$S = -k_B/e \ln((2-c)/c)$$

where k_B, e and c are respectively the Boltzmann constant, the charge of an electron and the site occupancy. According to Heikes model, the Seebeck coefficient reaches a constant value at high temperature. In $La_7Mo_7O_{30}$, the Seebeck coefficient varies little from 138 $\mu V/K$ at 350K up to 152 μVK^{-1} at 1000K with an uncertainty of 6 μVK^{-1}. This leads to calculated site occupancies of 0.33 and 0.29 at respectively 350K and 1000K. In $La_7Mo_7O_{30}$, there are two molybdenum sites with an average valence of +4.5 and +5.75 corresponding to respectively a site occupancy of 0.5 and 0.25 [50]. The site occupancy close to 0.3 indicates that the charge carrier is related to the hopping of molybdenum V to molybdenum VI corresponding to the more distorted sites [50].

The power factor increases from 1.10^{-7} $Wm^{-1}K^{-2}$ at room temperature to $2.5.10^{-5}$ $Wm^{-1}K^{-2}$ at 1000 K (figure 6). The thermal conductivity (Figure 7) is extremely low and decreases slightly with temperature from 0.77 to 0.58 $Wm^{-1}K^{-1}$. The thermal conductivity of $La_7Mo_7O_{30}$ is similar to the thermal conductivity of $La_2Mo_2O_9$[43, 44]. Therefore, a figure of merit of 0.04 is reached at 1000 K (figure 8).

The value of the ZT is quite encouraging. Indeed, the three most studied n-type thermoelectric oxides are $SrTiO_3$, ZnO, and $CaMnO_3$. In the first article, concerning the thermoelectric properties of $CaMnO_3$, a Seebeck coefficient of -100 μVK^{-1} and an electrical conductivity around 10000 Sm^{-1} (corresponding to activation energy of 0.16 eV) were reported [13]. The ZT value obtained was 0.08. By changing and optimizing the doping, ZT values higher than 0.3 were reached in $CaMnO_3$ [14]. In the case of ZnO, a Seebeck coefficient close to -180 μVK^{-1} and an electrical conductivity of 3 10^4 Sm^{-1} led to a ZT value of 0.24 at 1000K [12]. With dually doped ZnO, a ZT value of 0.47 at 1000 K was reported [62]. In the case of La-doped SrTiO3, single crystals exhibited an electrical conductivity of 10^6 Sm^{-1} and a Seebeck value of -150 μVK^{-1} leading to a ZT value of 0.08 [26]. With appropriate doping and composite approach, a ZT value higher than 1 has been reported [33]. $La_7Mo_7O_{30}$ exhibits a Seebeck coefficient close to those observed in these state-of-the-art n-type oxides. However, the value of electrical conductivity is too low to achieve similar power factors. Nevertheless, $La_7Mo_7O_{30}$ is undoped and the electrical conductivity can be clearly improved by doping, allowing for a substantial increase in ZT value.

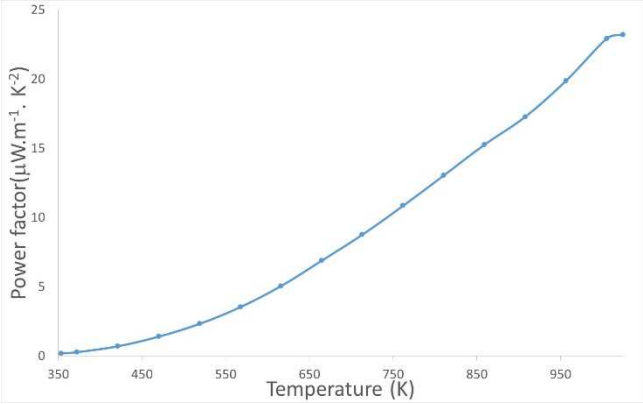

Figure 6: Power factor of $La_7Mo_7O_{30}$ ceramic versus temperature.

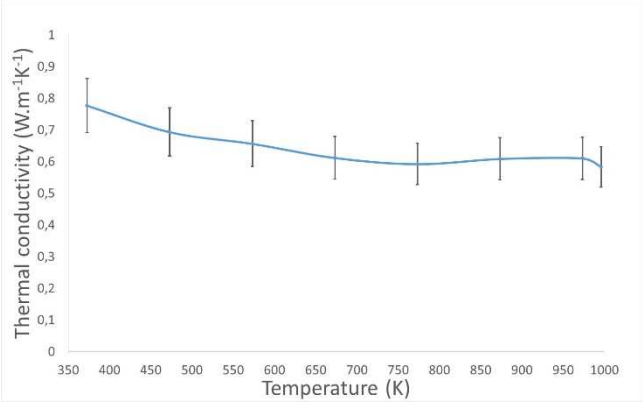

Figure 7: Thermal conductivity of $La_7Mo_7O_{30}$ ceramic versus temperature.

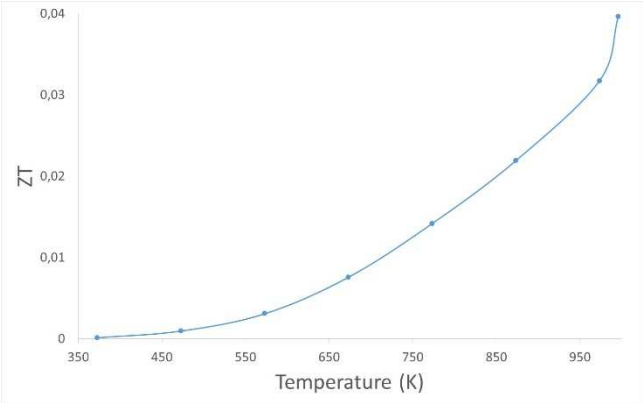

Figure 8: ZT value of $La_7Mo_7O_{30}$ ceramic versus temperature.

Conclusion

Spark plasma sintering of $La_2Mo_2O_9$ powder has been used to achieve $La_7Mo_7O_{30}$ ceramics. With a sintering time of 10 minutes at 973 K and an applied pressure of 90 MPa, a partial reduction of $La_2Mo_2O_9$ is observed and after 30 minutes, the reduction of $La_2Mo_2O_9$ is almost completed. Electrical conductivity of the $La_7Mo_7O_{30}$ ceramic exhibits a semiconducting behaviour and reaches 1000 Sm^{-1} at 1000 K. The negative Seebeck coefficient shows a n-type conduction. This ceramic exhibits a very low thermal conductivity, lower than 1 $Wm^{-1}K^{-1}$ from room temperature up to 1000 K and similar to values reported for $La_2Mo_2O_9$. A figure of merit of 0.04 is obtained for 89 % relative density bulk samples with remaining traces of $La_2Mo_2O_9$. It should then be possible to improve the power factor of these samples by increasing their relative density and removing the $La_2Mo_2O_9$ impurity. These first property measurements on the compound $La_7Mo_7O_{30}$ strongly encourage its study as a potential thermoelectric material. Indeed, substitutions would have to be considered to optimise transport properties and reduce thermal conductivity of $La_7Mo_7O_{30}$ ceramics.

References

[1] J.W. Fergus, Oxide materials for high temperature thermoelectric energy conversion, J. Eur. Ceram. Soc. 32 (2012) 525–540.

[2] M.W. Gaultois, T.D. Sparks, C.K.H. Borg, R. Seshadri, W.D. Bonificio, D.R. Clarke Data-driven review of thermoelectric materials : performance and resource considerations, Chem. Mater. 25 (2013) 2911-2920.

[3] I. Terasaki, Y. Sasago, K. Uchinokura, Large thermoelectric power in $NaCo_2O_4$ single crystals, Phys. Rev. B. 56 (1997) R12685-R12687.

[4] M. Shikano, R. Funahashi, Electrical and thermal properties of single-crystalline $(Ca_2CoO_3)_{0.7}CoO_2$ with a $Ca_3Co_4O_9$ structure, Appl. Phys. Lett. 82 (2003) 1851-1853.

[5] A. Sotelo, E. Guilmeau, M. A. Madre, S. Marinel, S. Lemmonier, J. C. Diez, $Bi_2Ca_2Co_{1.7}O_x$ Thermoelectric Ceramics Textured by Laser Floating Zone Method, Bol. Soc. Esp. Ceram. Vidrio 47 (2008) 225-228.

[6] F. Delorme, C. Chen, B. Pignon, F. Schoenstein, L. Perriere, F. Giovannelli, Promising high temperature thermoelectric properties of dense Ba2Co9O14 ceramics, J. Eur. Ceram. Soc. 37 (2017) 2615-2620.

[7] J. Androulakis, P. Migiakis, J. Giapintzakis, $La_{0:95}Sr_{0.05}CoO_3$, An efficient room-temperature thermoelectric oxide, Appl. Phys. Lett. 84 (2004) 1099-1101.

[8] M.A. Bousnina, R. Dujardin, L. Perriere, F. Giovannelli, G. Guegan, F. Delorme, Synthesis, sintering, and thermoelectric properties of the solid solution $La_{1\_x}Sr_xCoO_3$. J. Adv. Ceram. 7 (2018) 160-168.

[9] C. Chen, F. Delorme, F. Schoenstein, M. Zaghrioui, D. Flahaut, J. Allouche, F. Giovannelli, Synthesis, sintering and thermoelectric properties of $Co_{1-x}M_xO$. J. Eur. Ceram. Soc. 39 (2019) 346-351.

[10] K. Koumoto, H. Koduka, W-S Seo, Thermoelectric properties of single crystal $CuAlO_2$ with a layered structure. Journal of Materials Chemistry 11 (2001) 251-252.

[11] Y. Liu, Y-H. Lin, B-P. Zhang, H-M. Zhu, C-W. Nan, J. Lan, J-F Li, High-temperature thermoelectric properties in the $La_{2-x}R_xCuO_4$ (R : Pr, Y, Nb) ceramics, J. Am. Ceram. Soc. 92 (2009) 934-937.

[12] M. Ohtaki, T. Tsubota, K. Eguchi, H. Arai, High-temperature thermoelectric properties of $(Zn_{1-x}Al_x)O$, J. Appl. Phys. 79 (1996) 1816-1818.

[13] M. Ohtaki, H. Koga, T. Tokunaga, K. Eguchi, H. Arai, electrical transport properties and high temperature thermoelectric performances of $Ca_{0.9}(M_{0.1})MnO_3$ (M= Y, La, Ce, Sm, In, Sn, Sb, Pb, Bi). J Solid State Chem, 120 (1995) 105

[14] L. Bocher, M. Aguirre, D. Logvinovich, A. Shkabko, R. Robert, M. Trottmann,A. Weidenkaff, $CaMn_{1-x}Nb_xO_3$ (x = 0.08) perovskite-type phases as promising new high-temperature n-type thermoelectric materials, Inorg.Chem. 47 (2008) 8077-8085.

[15] C. Chen, F. Giovannelli, J. Duclère, F. Delorme - Thermoelectric properties of $Fe_2(Ti_{1-x}Nb_x)O_5$ pseudobrookite ceramics with low thermal conductivity - J. Eur. Ceram. Soc. 37(2017) 4681-4685.

[16] F. Azough, R. Freer, S.R. Yeandel, J. D. Baran, M. Molinari, S.C. Parker, E. Guilmeau, D. Kepaptsoglou, Q. Ramasse, A. Knox, D. Gregory, D. Paul, M.Paul, A. Montecucco, J. Siviter, P. Mullen, W. Li, G. Han, E.A. Man, H. Baig, T. Mallick, N. Sellami, G. Min, T. Sweet, $Ba_{6-3x}Nd_{8+2x}Ti_{18}O_{54}$ Tungsten Bronze: A new high-temperature n-type oxide thermoelectric, J. Electron. Mater. 45 (2016) 1894-1899.

[17] E. Guilmeau, D. Berardan, C. Simon, A. Maignan, B. Raveau, D. Ovono Ovono, F. Delorme, Tuning the transport and thermoelectric properties of In_2O_3 bulk ceramics through doping at In-site, J. Appl. Phys. 106 (2009) 053715, pp 1-7.

[18] Q. He, Q. Hao, G. Chen, B. Poudel, X. Wang, D. Wang, Z. Ren, Thermoelectric property studies on bulk TiO_x with x from 1 to 2, Appl. Phys. Lett. 91 (2007) 052505

[19] P. Thiel, S. Populo, S. Yoon, A. Weidenkaff, Enhancement of redox-and phase-stability of thermoelectric $CaMnO_{3-\delta}$ by substitution, J. Solid State Chem. 229 (2015) 62–67.

[20] X. Xiao, M. Widenmeyer, W. Xie, T. Zou, S.Yoon,M. Scavini, S. Checchia, Z. Zhong, P. Hansmann, S. Kilper, A. Kovalevsky, A. Weidenkaff, Tailoring the structure and thermoelectric properties of BaTiO3 via Eu^{2+} substitution, Phys. Chem. Chem. Phys., 2017, 19, 13469—13480.

[21] Y. Hirose, M. Tsuchii, K. Shigematsu, Y. Kakefuda, T. Mori, T. Hasegawa, Thermoelectric properties of amorphous ZnO_xN_y thin films at room temperature, Appl. Phys. Lett. 114 (2019) 193903-193907

[22] H. Son, Q. Guo, Y. Suzuki, B. Kim, T. Mori, Thermoelectric properties of MgTi 2 O 5 /TiN conductive composites prepared via reactive spark plasma sintering for high temperature functional applications, Scripta Materialia 178 (2020) 44–50.

[23] S. Ning, S.Huang, Z. Zhang, B. Zhao, R. Zhang, N. Qia, Z. Chen, β-Ga_2O_3: a potential high-temperature thermoelectric material, Phys. Chem. Chem. Phys. 24 (2022) 12052-12062.

[24] I. Sinnarasa, Y. Thimont, L Presmanes, A. Barnabé, P. Tailhades, Thermoelectric and transport properties of delafossite $CuCrO_2$:Mg thin films prepared by RF magnetron sputtering, Nanomaterials 7 (2017) 157-172.

[25] H. Alam, S. Ramakrishna, A review on the enhancement of figure of merit from bulk to nanothermoelectric materials. Nano Energy 2 (2013) 190–212.

[26] S. Ohta, T. Nomura, H. Ohta, K. Koumoto, High-temperature carrier transport and thermoelectric properties of heavily La- or Nb-doped $SrTiO_3$ single crystals. J. Appl. Phys. 97 (2005) 034106.

[27] C. Chen, M. Bousnina, F. Giovannelli, F. Delorme, Influence of Bi on thermoelectric properties of $SrTiO_{3-\delta}$, J. of Materiomics 5 (2019) 88-93.

[28] A.M. Dehkordi, S. Bhattacharya, J. He, H.N. Alshareef, T.M. Tritt, Significant enhancement in thermoelectric properties of polycrystalline Pr-doped $SrTiO_3$ ceramics originating from non uniform distribution of Pr dopants. Appl. Phys. Lett. 104 (2014) 193902.

[29] K. Koumoto, Y. Wang, R. Zhang, A. Kosuga, R. Funahashi, Oxide Thermoelectric Materials: A Nanostructuring Approach, Ann. Rev. Mater. Res. 40 1(2010) 363-394

[30] F. Delorme, R. Dujardin, F. Schoenstein, B. Pintault, P. Belleville, C. Autret, I. Monot-Laffez, F. Giovannelli, Nanostructuring of dense SnO_2 ceramics by Spark Plasma Sintering, Ceramics International 45 (2019) 8313-8318.

[31] T. Loland, J. Sele, M. Einarsrud, P. Vullum, M. Johnsson, K. Wiik, Thermal conductivity of A-site cation deficient La-Substituted $SrTiO_3$ produced by Spark Plasma Sintering; Energy Harvesting and systems 2 (2015) 63-71.

[32] F. Giovannelli, C. Chen, P. Diaz-Chao, E. Guilmeau, F. Delorme - Thermal Conductivity and Stability of Al-doped ZnO nanostructured ceramics - J. Eur. Ceram. Soc. 38 (2018) 5015-5020.

[33] M. Acharya, S. Sourav Jana, M. Ranjan, T. Maiti, High performance (ZT>1) n-type oxide thermoelectric composites from earth abundant materials, Nano Energy 84 (2021) 105905.

[34] F. Delorme, P. Diaz-Chao, E. Guilmeau, F. Giovannelli, Thermoelectric properties of Ca3Co4O9–Co3O4 composites, Ceram. Int. 41 (2015) 10038-10043.

[35] D. Srivastava, C. Norman, F. Azough, M.C. Schäfer, E. Guilmeau, R. Freer, Improving the thermoelectric properties of SrTiO3-based ceramics with metallic inclusions, J. Alloys Compoud. 731 (2018) 723-730.

[36] Y. Saito, T. Matsuno, Q.Guo, T. Mori, M. Kashiwagi,A. Shimojima, H. Wada, K.Kuroda, Preparation of ordered nanoporous indium tin oxides with large crystallites and individual control over their thermal and electrical conductivities, Appl. Mater. Interfaces 13 (2021) 15373–15382.

[37] R.Virtudazo, B. Srinivasan, Q.Guo, R. Wu, T. Takei, Y. Shimasaki, H. Wada, K. Kuroda, S. Bernik, T. Mori, Improvement in the thermoelectric properties of porous networked Al-doped ZnO nanostructured materials synthesized via an alternative interfacial reaction and low-pressure SPS processing Inorg. Chem. Front. 7 (2020) 4118-4132.
[38] S. Saini, P. Mele, T. Oyake, J. Shiomi, J.Niemela, M. Karppinen, K. Miyazaki, C. Li, T. Kawaharamura, A. Ichinose,L. Molina-Luna, Porosity-tuned thermal conductivity in thermoelectric Al-doped ZnO thin films grown by mist-chemical vapor deposition, Thin Solid Films 685 (2019) 180–185.

[39] H. Kaga, R. Asahi, T. Tani, Thermoelectric Properties of Doped (ZnO)mIn_2O_3 Jap. J. Appl. Phys. 43 (2004)3540-3543.

[40] Y. Michiue, H. Nishijima, Y Suzuki, T. Mori, Synthesis and thermoelectric properties of composite oxides in the pseudobinary system ZnO-Ga_2O_3, Solid State Sciences 65 (2017) 29-32.

[41] Y. Michiue, T. Mori, A. Prytuliak, Y. Matsushita, M. Tanaka, N. Kimizuka, Electrical, optical, and thermoelectric properties of $Ga_2O_3(ZnO)_9$, RSC Advances, 2011, 1, 1788–1793.

[42] E. Guilmeau, P. Díaz-Chao, O. Lebedev, A. Recnik, M. Schafer, F. Delorme, F. Giovannelli, M. Kosir, and S. Bernik – Inversion boundaries and phonon scattering in Ga:ZnO thermoelectric compounds- Inorg Chem. 2017, 56, 480-487

[43] M. R. Winter, D. R. Clarke, Oxide Materials with Low Thermal Conductivity. J. Am. Ceram. Soc. 90 (2007) 533–540.

[44] E. Sabarthes, F. Delorme, V. Tezyk, C. Autret, G. Corbel, P. Lacorre, F. Giovannelli, Reducing the thermal conductivity of $La_2Mo_2O_9$ with a trivalent praseodymium substitution for its potential use as a thermal barrier coating, Dalton Trans. 48 (2019) 10051- 10061.

[45] C. Li, Q.F. Fang, Internal friction study of oxygen ion conductors $La_{1.95}K_{0.05}Mo_{2-x}T_xO_{9-\delta}$ (T = Fe,Mn), J. Appl.Phys. 101 (2007) 083508.

[46] I.P Marozau, D Marrero-López, A.L Shaula, V.V Kharton, E.V Tsipis, P Núñez, J.R Frade. Ionic and electronic transport in stabilized β-$La_2Mo_2O_9$ electrolytes. Electrochimica Acta 49 (2004) 3517–3524.

[47] S. Lee, G. Yang, R.H.T.Wilke, S. Trolier-McKinstry, C. A. Randall, Thermopower in highly reduced n-type ferroelectric and related perovskite oxides and the role of heterogeneous nonstoichiometry, Phys. Rev. B 79 (2009) 134110.
[48] P. Lacorre, F. Goutenoire, Odile Bohnke, R. Retoux, Y. Laligant _ Designing fast oxide-ion conductors based on $La_2Mo_2O_9$ -Nature 404 (2000) 856-858

[49] Vega-Castillo, J. E.; Ravella, U. K.; Corbel, G.; Lacorre, P.;Caneiro, A. On the local order of amorphous $La_2Mo_2O_{6.7}$, Dalton Trans. 41 (2012) 7266−7271.

[50] F. Goutenoire, R. Retoux, E. Suard, P. Lacorre, Ab Initio determination of the novel perovskite-related structure of $La_7Mo_7O_{30}$ from Powder Diffraction, J. Solid State Chem. 142 (1999) 228–235.

[51] A. Shakouri, Recent Developments in semiconductor thermoelectric physics and materials, Annu. Rev. Mater. Res. 41 (2011) 399–431.

[52] S. Walia, S. Balendhran , H. Nili,S. Zhuiykov , G.Rosengarten, Q.Wang, M. Bhaskaran, S. Sriram, M. S. Strano , K. Kalantar-zadeh- Transition metal oxides – Thermoelectric properties. Prog. Mater. Sci. 58, 1443–1489 (2013).

[53] G. Buvat, H. Sellemi, U. K. Ravella, M. Barré, S. Coste, G. Corbel, P. Lacorre, Reduction kinetics of $La_2Mo_2O_9$ and phase evolution during reduction and reoxidation, Inorg. Chem. 55 (2016) 2522–2533.

[54] J. Vega-Castillo, L. Mogni, G. Corbel, P. Lacorre and A. Caneiro, On the thermodynamic stability of La2Mo2O9−δ oxide-ion conductor, Int. J. Hydrogen Energy 35 (2010) 5890–5894.

[55] F. Delorme, M. Bah, F. Schoenstein, F. Jean, M .Zouaoui Jabli, I. Monot-Laffez, F. Giovannelli - Thermoelectric properties of oxygen deficient $(K_{0.5}Na_{0.5})NbO_3$ ceramics- Material letters 162 (2016) 24-27.

[56] Felix Kaiser, Paul Simon, Ulrich Burkhardt, Bernd Kieback, Yuri Grin and Igor Veremchuk, Spark Plasma Sintering of Tungsten Oxides WO_x ($2.50 \leq x \leq 3$): Phase Analysis and Thermoelectric Properties, Crystals 7 (2017) 271.

[57] P. Lacorre, A. Selmi, G. Corbel, B. Boulard, On the flexibility of the structural framework of cubic LAMOX compounds, in relationship with their anionic conduction properties, Inorg. Chem. 45 (2006) 627-635.

[58] I. Monot-Laffez, R. Retoux, M. Zaghrioui, M. Bah, F. Dorvaux, M. Dubernet, F. Delorme, F. Giovannelli- Microstructural features and piezoelectric properties of spark plasma sintered lead-free $K_{0.5}Na_{0.5}NbO_3$ ceramics - Eur. Phys. J. Spec. Top. (2022). https://doi.org/10.1140/epjs/s11734-022-00573-y

[59] I.G. Austin, N.F Mott, Polarons in Crystalline and Non Crystalline Materials, Adv. in Physics 18 (1969) 41-102.

[60] Chaikin P.M., Beni G. Thermopower in the correlated hopping regime Phys Rev B 13 (1976) 647-651.

[61] S.D. Kang, M. Dylla, G. J. Snyder, Thermopower-conductivity relation for distinguishing transport mechanisms : polaron hopping in CeO_2 and band conduction in $SrTiO_3$, Phys rev B 97(2018) 235201.